

Kv4 (A-type) Potassium Currents in the Mouse Medial Nucleus of the Trapezoid Body

By Jamie Johnston^{1,2}, Sarah J. Griffin¹, Claire Baker¹ and Ian D. Forsythe¹.

Addresses: MRC Toxicology Unit¹ and Department of Cell Physiology & Pharmacology², University of Leicester, Leicester LE1 9HN, UK.

JJ current address: Department of Biology, University of Victoria, British Columbia, Canada

Correspondence to: Professor Ian D. Forsythe, MRC Toxicology Unit, University of Leicester, Leicester LE1 9HN, UK. Fax: +44 (0)116 252 5616, email: idf@le.ac.uk

Running title: Kv4 in the MNTB

Pages: 24

Figures: 5

Tables: 2

Equations: 4

Words: Total 5516, Abstract 141, Introduction 393

Keywords: K⁺ channel, **Hodgkin-Huxley model**, **voltage-clamp**, **current clamp**, **auditory processing**.

Abstract

Principal neurones of the mouse medial nucleus of the trapezoid body (MNTB) possess multiple voltage-gated potassium currents, including a transient outward current (or A-current) which is characterised here. The A-current exhibited rapid voltage-dependent inactivation and was half-inactivated at resting membrane potentials. Following a hyperpolarising pre-pulse to remove inactivation, the peak transient current was 1.07 nA at -17 mV. The pharmacological characteristics of this A-current were consistent with Kv4 subunits in expression studies; the A-current was resistant to block by tetraethylammonium and dendrotoxin-I, but sensitive to millimolar concentrations of 4-aminopyridine and 5 μ M hanatoxin. Immunohistochemistry confirmed that Kv4.3 subunits are present in the MNTB. In a single-compartment model of an MNTB neurone, the A-current served to accelerate the decay of the **initial** action potentials in a **stimulus** train and **suggested that removal of A-current steady-state inactivation could** raise firing threshold for non-calyceal synaptic inputs. **This A-type current was not observed in the rat.**

Introduction

Excitability is controlled across many different neuronal types by expression of variable suites of potassium channels from up to 12 different gene families {Coetzee, 1999 #6}. Although recombinant homomeric channels are well characterised, the specific roles of many native ion channels in identified neurones has still to be elucidated. The principal neurones of the medial nucleus of the trapezoid body (MNTB) are an attractive preparation for studying native K⁺ channels, since these relatively compact neurones facilitate good voltage control, {Brew, 1995 #7; Brew, 2007 #17; Brew, 2003 #10; Dodson, 2002 #8; Kaczmarek, 2005 #21; Klug, 2006 #22; Wang, 1998 #23}. The MNTB functions as an inverting relay in the auditory brainstem circuits underlying the physiological mechanisms of sound source localisation {Masterton, 1967 #42}. This function requires temporally accurate transmission of AP firing in the pre-synaptic neurone to AP firing in the MNTB principal neurone. While the giant calyx of Held synapse assists security of transmission, the magnitude of the EPSC requires precise expression of voltage-gated potassium channels to suppress hyper-excitability {Dodson, 2002 #8; Schleggenburger, 2006 #44} Kv1 potassium channels are responsible for suppression of excitability at voltages around the action potential (AP) threshold; while Kv3 potassium channels mediate rapid AP repolarisation and hence promote high frequency firing {Brew, 1995 #7; Wang, 1998 #23}. Together, these currents allow the postsynaptic neurone to follow the pattern of AP firing of the major synaptic input (the calyx of Held).

MNTB neurones also possess other potassium currents, including a transient outward potassium current or A-current. A-type K⁺ currents are expressed at several sites along the auditory pathway, including: type II spiral ganglion neurones {Jagger, 2003 #29}, a subpopulation of Type I cells of the ventral cochlear nucleus {Rothman, 2003 #28}, lateral **olivocochlear** (LOC) neurones of the lateral superior olive {Fujino,

1997 #31} and in the dorsal nucleus of the lateral lemniscus {Fu, 1996 #26}. In this paper we characterise an A-type current in mouse MNTB. We demonstrate that principal neurones possess a small, rapidly inactivating A-current mediated by Kv4 subunits. We assess the significance of this current by modelling its contribution to MNTB whole cell currents. At resting membrane potentials, it is largely inactivated but, following hyperpolarisation which removes inactivation, it may serve to accelerate AP time-course. Intriguingly, rat MNTB neurones do not possess this current.

Materials and Methods

Electrophysiology: Brainstem slices (120-150 μ m thick) were prepared as described previously {Dodson, 2002 #8}. Briefly, 10-14 or 18-19 day CBA mice were killed by decapitation in accordance with the UK animals (Scientific Procedures) Act 1986. The brainstem was mounted on the stage of an Integraslice (Campden Instruments, **Loughborough, UK**) and transverse slices cut in a low-sodium artificial cerebrospinal fluid (aCSF) at around 0 $^{\circ}$ C. Subsequently, slices were incubated at 37 $^{\circ}$ C in normal aCSF for one hour, and were then allowed to cool to room temperature. For recording, one slice was placed in the environmental chamber on the stage of a Nikon FN600 microscope and perfused with aCSF (\sim 1ml min $^{-1}$ at 25-27 $^{\circ}$ C). Whole-cell patch recordings were made from visually identified neurones in the MNTB using an Optopatch amplifier (Cairn, **Faversham, UK**). Patch pipettes (borosilicate glass, GC150F-7.5, Harvard Apparatus, **Edenbridge, UK**) ***contained a solution of composition (in mM) 97.5 K-Gluconate, 32.5 KCl, 10 HEPES, 5 EGTA, 0.01 ZD 7288 (was included in voltage-clamp recordings to block I_h) and 1 MgCl₂ (pH 7.2 with KOH).*** Patch pipettes had series resistances of 4-12M Ω and were compensated by at least 75% with 10 μ s lag. A holding potential of -77mV was used under voltage-clamp and neurones under current clamp were held at between –

67mV and -77 mV; recordings were excluded from analysis if >250pA of current was required to do this. The normal aCSF contained (in mM): 125 NaCl, 2.5 KCl, 10 Glucose, 1.25 NaH₂PO₄, 2 sodium pyruvate, 3 myo-inositol, 0.5 ascorbic acid, 0.5 CaCl₂ and 2.5 MgCl₂. The low-sodium aCSF contained (in mM): 2.5 KCl, 10 Glucose, 1.25 NaH₂PO₄, 26 NaHCO₃, 250 sucrose, 0.5 ascorbic acid, 0.1 CaCl₂, and 3.9 MgCl₂. All aCSFs were bubbled with 95%O₂/5%CO₂ giving a pH of 7.4.

Data acquisition and analysis: The majority of data were collected from P10-14 animals, **with an additional** 5 cells from P18-19 animals. Data were acquired using pClamp 9.2 and a Digidata 1322A interface (Molecular Devices) filtered at 2-5kHz and digitised at 10-50kHz. All voltages were corrected for a -7mV junction potential and no leak subtraction was performed. Data are presented as means ±SEM and a two-tailed Student's t-test (paired or unpaired) was used to assess significance. Activation and inactivation parameters were determined by a Boltzmann function of the form $I = I_{\max} / (1 + e^{(V - V_{1/2})/k})$ with variables I_{\max} , $V_{1/2}$ and k (the slope factor). For activation of the A-current, the peak amplitude from the I/V was corrected for non-linearity of the single channel current using a modified GHK equation of the form $i = \alpha * ((F^2V)/(RT)) * ([K^+]_{in} - [K^+]_{out} * e^{-(FV/RT)}) / (1 - e^{-(FV/RT)})$ where symbols have their usual meaning and α is a normalisation factor {Clay, 2000 #2}. For comparison of the relative contributions from K⁺ channels, the chord conductance was used, that is $G = I / (V - E_K)$. Exponential fits were performed using Clampfit 9.2 (Molecular Devices) or Excel (Microsoft) with least squares minimisation.

Immunohistochemistry: P13 CBA mice brainstems were frozen in Tissue Tek (Sakura) using hexane and dry ice. *Unfixed tissue was sectioned, so that antibodies could be tested in four different fixation conditions: the four conditions were: 4%*

*paraformaldehyde (PFA), PFA with antigen retrieval, methanol and methanol with antigen retrieval. PTA, without antigen retrieval was selected as giving the most specific staining (on the basis of low background; competition by blocking peptide and overall staining intensity) for all of the three Kv4 antibodies. This method is similar to that reported previously {Dodson, 2003 #1; Dodson, 2002 #8}. Cryostat sections (12µm) were mounted on polylysine-coated slides and fixed in 4% paraformaldehyde/PBS for 25min at 4°C. After washing 3x5 minutes in 100mM PBS with 0.1% Triton X-100 (PBS-T), **those slides receiving 'antigen retrieval'** were treated with citrate buffer (pH6.0) for 20min at 95°C. After rewashing in PBS-T, sections were blocked with 1% BSA and 1% goat serum in PBS-T for 1h at 20°C and then incubated with anti-Kv4 antibodies (Sources: Kv4.1Ab: Santa Cruz, C-18 Sc-16025, 1:100; Kv4.2Ab & Kv4.3Ab, Alomone Labs, APC-023 and APC-017, respectively; at 1:800) in blocking buffer overnight at 4°C. After washing with PBS-T, the secondary antibody (goat anti-rabbit Alexa-fluor488, Molecular Probes, 1:1000) was applied for 2hr at 20°C, then mounted with Vectashield (Vector Labs., **Peterborough UK**). Images were obtained using a Leica fluorescence microscope (DM2500) fitted with a CCD camera (Leica, DFC350Fx). Control sections underwent identical procedures, but in the presence of blocking peptide.*

Solutions and drugs: All chemicals were obtained from Sigma-Aldrich, UK (except: TTx (Latoxan, **Blum France**), dendrotoxin-I (Alomone, **Jerusalem Israel**), ZD7288 (Tocris Cookson, **Bristol UK**), and Alexa-fluor (goat-anti-rabbit) (Molecular Probes, **Invitrogen, Paisley UK**). Hanatoxin was a kind gift from Dr. K Swartz [NINDS, NIH, USA).

Modelling: Isolated A-currents were fit (by minimising the sum of the squared error using Matlab (The Mathworks Inc, USA) with a Hodgkin-Huxley model of the form,

$$I = A * GHK(v) * m^4 * z \quad (\text{equation 1})$$

where A dictated the magnitude of the conductance (and was a free parameter of the fit), GHK specified the Goldman-Hodgkin-Katz dependence on voltage, m was the activation variable, z was the inactivation variable and v was voltage.

For a voltage step from a negative voltage (assuming no activation and complete removal of inactivation) equation 1 took the form,

$$I = A * GHK * ((\text{minf}^{1/4} * (1 - \exp(-t/\text{mtau})))^4 * (\text{zinf} - (\text{zinf} - 1) * \exp(-t/\text{zhtau}))) \quad (\text{equation 2})$$

Where minf was the steady-state activation and zinf was the steady-state inactivation (both given by the Boltzman fits shown in Figure 1B), mtau was the time constant of activation and ztau was the time constant of inactivation (both free parameters in the fit) and t was time. The values of mtau and ztau are given in Table 1.

(Table 1 should appear near here)

The single-compartment MNTB model {Macica, 2003 #40} obtained from Model DB {Hines, 2004 #41} was manipulated using the NEURON simulation software {Hines, 2001 #32}. The reversal potential of the leak current, and therefore the resting membrane potential, was set to -80mV and the A-current model was incorporated. Synaptic currents were constructed using a reversal potential of 0 mV and were of the form:

$$I = B * G_a * (v - 0) + C * G_b * (v-0) \quad (\text{equation 3})$$

Where v was voltage, G was conductance and B (and C) were given by,

$$X = s * (\exp(-t/\tau_{x2}) - \exp(-t/\tau_{x1})) \quad (X = B \text{ or } C) \quad (\text{equation 4})$$

Where s was a scaling factor set to normalise the maximum of X to 1, τ_{x1} was the rise time constant, τ_{x2} was the decay time constant and t was time. G , τ_{x1} and τ_{x2} are given in Table 2.

(Table 2 should appear near here)

Results

Whole-cell patch clamp recordings were made from visually identified MNTB neurones from P10-14 mice. Outward K^+ currents were measured under voltage-clamp conditions in the presence of tetraethylammonium (TEA) and dendrotoxin-I (DTx-I) to block $Kv3$ and $Kv1$ currents, respectively {Brew, 1995 #7; Dodson, 2002 #8; Wang, 1998 #23}. Under these conditions a transient outward current was observed upon depolarization to -17mV (Figure 1A, black square), provided a conditioning hyperpolarizing voltage step (to remove inactivation) preceded this test depolarization. The amplitude of the transient outward current, at -17mV , was $1.07 \pm 0.15\text{nA}$ ($n=8$, from a conditioning voltage step to -117 mV , grey trace). This current inactivated rapidly, characteristic of an A-type potassium current {Connor, 1971 #33}. Steady-state inactivation was determined by stepping the conditioning voltage from -117 to -37mV and measuring the current evoked at -17 mV (Figure 1A, black square). The inactivation data were normalized and fit with a Boltzmann function

(Figure 1B, filled squares) with a half-inactivation ($V_{1/2in}$) of -76.9 ± 0.9 mV and a slope factor (k_{in}) of 7.0 ± 0.3 ($n=9$).

Activation was measured by comparing currents evoked during two test protocols shown in Figure 1C. Each test voltage (T1 & T2) was preceded by hyperpolarisation to -117 mV (to remove inactivation) but in T2, the A-current was inactivated by a pre-pulse to -37 mV for 20 ms. Subtraction of the T2 currents from the T1 currents gave the isolated A-current, shown in Figure 1D. The peak A-current was measured, adjusted to account for GHK rectification (see methods) and normalized (Figure 1B, closed circles). The activation data were fit with a Boltzmann function with a half-activation ($V_{1/2ac}$) of -35.0 ± 1.3 mV and slope factor (k_{ac}) -6.7 ± 0.3 , (Figure 1B, filled circles, $n=9$). At positive voltages rectification was observed, consistent with voltage-dependant block by $[Mg^{2+}]_i$ {Forsythe, 1992 #9; Slesinger, 1993 #12} so these points were excluded from the fit.

The isolated A-currents inactivated with a single exponential time-constant of 6.28 ± 0.77 ms (at -17 mV, $n=7$). To assess the rate of recovery from inactivation, a double pulse protocol was used, in which two -17 mV pulses were separated by a variable recovery period, as shown in Figure 1E. The A-current recovered completely in less than 50 ms with a single-exponential time course of $\tau = 16.4 \pm 1.6$ ms ($n=8$).

In 5 neurones from older animals (P18-19) the peak A-current at -17 mV was similar to data obtained at P10-P14, with an amplitude of 1.2 ± 0.15 nA ($n=5$). Inactivation Boltzmann parameters were also similar ($k = 7.6$, $V_{1/2in} = -77.2$, $n=5$) and the inactivation time constant measured at -17 mV was not significantly different between the two age groups ($\tau = 7.7$ ms, $p=0.23$).

Pharmacology of the A-current

Kv1, Kv3 and Kv4 potassium channel families possess subunits with A-type characteristics {Coetzee, 1999 #6}. We used a pharmacological approach to dissect which subunits mediated the A-current observed here. Kv3 channels are eliminated

since they are all sensitive to micromolar concentrations of TEA {Rudy, 2001 #18} and the A-current was still present in 100mM TEA (substituted for NaCl, n=3, Figure 2A).

Although Kv1 channels are largely insensitive to millimolar concentrations of TEA, our recordings were made in the presence of dendrotoxin-I, which blocks Kv1 currents in MNTB neurones {Brew, 1995 #7; Dodson, 2002 #8}. It is theoretically conceivable that DTx-insensitive Kv1 channels composed of Kv1.3 or Kv1.4 could form an inactivating outward current. However CP 339,818 (5-10 μ M), an antagonist of Kv1.3 and Kv1.4 channels {Jager, 1998 #14; Nguyen, 1996 #13}, had no effect on the A-current (n=3, data not shown, recorded in TEA & DTx-I).

Kv4 subunits are resistant to TEA and are blocked by 4-aminopyridine (4-AP) {Coetzee, 1999 #6}. The A-current in the MNTB was largely blocked by 4-AP as shown in Figure 2B (5-10mM, n= 4, in the presence of TEA & DTx-I). Furthermore, local pressure ejection of 5 μ M hanatoxin from a puffer pipette reduced the maximum A-current measured at -17 mV by $68 \pm 13\%$ (Figure 2C, n=4). Hanatoxin selectively shifts the voltage-dependence of Kv4 (and Kv2.1) activation to more positive voltages {Swartz, 1995 #19}. Together these data are consistent with mediation of the MNTB A-current by Kv4 channels.

Kv4.3 protein is expressed in the MNTB

Kv4 subunits classically mediate A-type K⁺ currents {Birnbaum, 2004 #5}. To examine the expression of Kv4 subunits in the MNTB we used well-characterised antibodies against the three family members: Kv4.1, Kv4.2 and Kv4.3 {Amberg, 2002 #4; Kollo, 2006 #3}. There was robust staining above the blocking peptide control for Kv4.3, whereas staining for Kv4.2 was only just above background (Figure 3). **Similar to other Kv subunits, the Kv4.3 staining shows significant cytoplasmic staining with some indication of membrane localisation (Figure 3X, arrow) [add**

correct figure ref]. The presence of Kv4.3 is consistent with reports of Kv4.3 *in situ* hybridization in the MNTB {Lein, 2007 #39}. No specific staining above background was observed for Kv4.1, consistent with Kv4.1 only being expressed in the olfactory bulb and CA1 of the hippocampus {Fitzakerley, 2000 #15; Serodio, 1998 #16}.

Species differences

Although we found an A-current in every neurone tested in mouse MNTB (>30 cells), we did not detect an A-current in any of 6 MNTB neurones tested in the rat (Figure 2D). This finding is consistent with previous independent reports from mouse {Brew, 2003 #10} and rat {Dodson, 2002 #8}.

Physiological role

To investigate the physiological role of the A-current present in MNTB principal neurones, current clamp recordings were made before and after application of 5 μ M hanatoxin (which reduces the magnitude of the A-current at physiologically relevant voltages; see above). Action potentials were elicited by injection of depolarising current steps from holding potentials of -67 and -77 mV (chosen to reduce A-current inactivation), and AP characteristics (threshold, half-width and latency) were measured. However, no significant changes or trends in AP characteristics were **observed between control and hanatoxin treated cells [correct Jamie?]** (n=3, all p>0.05; paired t-tests).

The A-current is small relative to the magnitude of other K⁺ currents in the MNTB; when inactivation is removed by a hyperpolarising pre-pulse, there is **a maximum A-current of ~10 nS** available (calculated at -17mV) versus more than 55 nS from the other outward K⁺ currents (calculated at 13mV). At resting membrane potentials the A-current is more than half-inactivated (Figure 1B), reducing its contribution **to the overall outward conductance. So combined with its rapid time-course**, the

influence this A-current can exert on shaping the voltage response **is likely to be subtle and was difficult to resolve from direct patch recording**. Therefore, we used a modelling approach to test its contribution to MNTB neurone excitability. A Hodgkin-Huxley model was fit to isolated A-currents (Figure 4A) and the mean time constants for activation and inactivation, obtained from 5 such fits (see Table 1), were used to produce the final model MNTB A-current (Figure 4B). This was added to a single-compartment model (containing high and low voltage-activated potassium currents), which captures salient features of MNTB AP firing {Macica, 2003 #40; Song, 2005 #44; Wang, 1998 #23}.

The membrane potential response to a simulated 200 Hz train of 20 large synaptic currents (simulating transmitter release from the pre-synaptic Calyx of Held; see methods) is shown in Figure 5A. Data from the full model is shown in black, whereas the grey trace represents the voltage following complete removal of the A-current from the model. In response to this “calyceal” stimulus, APs were generated in response to each synaptic event and appeared qualitatively similar in the presence or absence of the A-current. The first AP (Figure 5B) was narrower when the model included an A-current but this effect declined with each AP and was negligible by the last AP in a train, consistent with inactivation of the A-current (Figure 5C). *This prediction was verified using patch recording, by evoking APs in response to 200Hz trains of current pulses (each having a synaptic waveform). The average response to a minimum of 10 stimuli were used to reduce noise. Under these conditions the first AP was found to have a halfwidth $30 \pm 5 \mu\text{s}$ shorter than the second AP ($n=4$, $p=0.01$, data not shown).*

Principal neurones in the MNTB also receive synaptic stimulation that is sub-threshold (or around threshold) particularly from non-calyceal inputs {Hamann, 2003 #24}. We reasoned that the A-current would have a more significant effect on MNTB

AP firing in response to stimulation that was just above threshold for AP firing. The slower time-course and small amplitude of the non-calyceal inputs would allow more of the A-current to activate before APs are generated. The MNTB model suggested that the A-current could influence AP firing in response to a non-calyceal synaptic stimulus (see methods; compare Figures 5D & E) despite the small magnitude of the A-current (Figure 5F), but this proved difficult to test in native neurons due to the variability induced by trial to trial quantal fluctuation.

Discussion

We have characterised a transient outward current in principal neurones of the MNTB. The kinetics and biophysical properties of this A-current are consistent with the Kv4 voltage-gated K⁺ channel family {Birnbaum, 2004 #5}. The pharmacology of the current, being insensitive to CP 339,818 and high concentrations of TEA, but blocked by 4-AP and hanatoxin is also consistent with data from recombinant Kv4 channels. Of the three Kv4 subunits, Kv4.3 exhibits significant *in situ* hybridization in the MNTB {Lein, 2007 #39} and antibodies to this subunit show robust labelling in principal neurones of the MNTB. It is likely that the channels mediating the fast A-current are predominantly composed of Kv4.3 subunits, perhaps with a minor contribution from Kv4.2, based on the low level staining (Figure 3).

The immunohistochemistry showed strong cytoplasmic labelling of Kv4.3, consistent with consistent with protein synthesis, trafficking or presence in other internal organelles. Some concentrations of Kv4.3 staining were also observed associated with the plasma membrane. In the hippocampus Kv4 currents are more highly expressed in dendritic rather than somatic compartments, where they participate in

synaptic plasticity {Johnston, 2003 #38}, MNTB neurones do possess small dendrites, but no specific staining of neuronal processes was observed.

A characteristic of this MNTB A-current is its rapid rate of inactivation, showing time-constants of less than 10ms *and fast recovery. This contrasts with heterologously expressed Kv4.3 subunits which have inactivation time constants of ~60-100ms* {Nadal, 2003 #41; Wang, 2002 #40}. *In general, A-currents of native neurons tend to have faster inactivation rates, although there is considerable variability between brain regions. Some have time-constants longer than 30ms; e.g. Locus coeruleus* {Forsythe, 1992 #9}; *VCN* {Rothman, 2003 #35} *and cortical pyramidal neurones* {Yuan, 2005 #36}. *Whereas, cerebellar granule neurons* {Bardoni, 1993 #43} *have similar rates to those in the MNTB. It is well established that Kv4 subunits are modulated by a plethora of accessory proteins and biochemical pathways* {Birnbaum, 2004 #5}. *Indeed it is likely that the faster kinetics of native A-currents versus their heterologously expressed counterparts is due to differences in accessory subunit expression* {An, 2000 #37; Birnbaum, 2004 #5; Nadal, 2003 #41; Rhodes, 2004 #42}. *[deleted and simplified the surrounding sentences] K⁺ channel interacting proteins (KChIP) are key candidates as they co-localise with Kv4.2 and Kv4.3 subunits in the mammalian brain* {Rhodes, 2004 #42}. *Although KChIPs speed recovery from inactivation they tend to slow inactivation* {Birnbaum, 2004 #5; Wang, 2002 #40}, *suggesting that other accessory subunits are required in the mouse MNTB, e.g. DPPX* {Nadal, 2003 #41} *and further work is required.*

Classically, A-currents increase inter-spike intervals, slowing firing rates and in the presence of suitable hyperpolarizing drive they contribute to oscillating firing {Connor, 1971 #33; Connor, 1971 #34}. The physiological roles of A-currents vary markedly in different parts of the auditory pathway. In the ventral cochlear nucleus the A-current modulates firing rate {Rothman, 2003 #27}, whereas in spiral ganglion neurones the

A-current is the dominant K^+ channel mediating action potential repolarisation {Jagger, 2002 #30}. These different roles reflect the varying channel kinetics and current densities relative to other K^+ channels in each neurone type.

MNTB principal neurones express high voltage-activated Kv3 channels that dominate action potential repolarisation {Brew, 1995 #7; Klug, 2006 #22; Wang, 1998 #23}. In comparison, the A-current is of relatively small magnitude, so it is not surprising that its effects on action potential repolarisation are modest. *Indeed both the model and our experimental data shows that the A-current makes only a tiny difference on the action potential half-width ($30\mu s$).* Nevertheless, such a small change could be significant for interaural comparison in the mouse, since their interaural distance is also small. The A-current is largely inactivated during sustained depolarisation but modelling showed that when the preceding membrane potential is hyperpolarised, the A-current can contribute to AP repolarisation during the first few action potentials of a train. At resting membrane potentials (-60 to $-70mV$) the A-current is more than half-inactivated. However, membrane hyperpolarisations of around $10mV$ raise the available A-current by ~ 2 fold (see Figure 1B). Such hyperpolarisations may occur after high frequency **stimulation** (as observed in the pre-synaptic terminal {Kim, 2007 #25}) or during inhibitory synaptic transmission. Indeed, with development, the MNTB receives a strong ($\sim 200nS$) glycinergic input {Awatramani, 2004 #11}, the role of which has yet to be determined. [Jamie – this is a bit repetitive of what has now been said elsewhere at the end of the results section so lets delete it here - Our modelling suggests that, since the A-current begins to activate just below action potential threshold (which is $-51.4 \pm 1.6mV$, $n=8$), a plausible mechanism for physiological activation of the A-current would be during integration of the small non-calyceal inputs {Hamann, 2003 #24}.]

An interesting limitation to the physiological function of this A-current is the rectification observed at positive membrane potentials. This is strongly reminiscent of voltage-dependent block by internal Mg^{2+} observed in unitary A-current channels {Forsythe, 1992 #9} and ShkB channels {Slesinger, 1993 #12} and will limit the magnitude of the A-current at the peak of the action potential.

A previous study reported a small 4-aminopyridine-sensitive A-current in mouse {Brew, 2003 #10}. However, there is no evidence for an A-current in the rat (Figure 2D) {Brew, 1995 #7; Dodson, 2002 #8}, suggesting an interesting species difference. It is difficult to speculate about the reasons for this species difference given that there is little information regarding binaural auditory processing in the mouse or rat (although sound localisation for free field stimuli has been investigated {Heffner, 1985 #45; Heffner, 1988 #47; Ehret, 1984 #48}). Based on the observations made here, the A-current would contribute to AP repolarisation at the onset of a sound stimulus, particularly following a hyperpolarising drive to MNTB neurones. In addition, it may contribute to integration of non-calyceal input to the MNTB, the origin and function of which are unknown. Therefore, the significance of this A-current for auditory processing in the mouse remains a question for further investigation.

Acknowledgements: Thanks to Kenton Swartz for the kind gift of purified hanatoxin. This work was funded by the Medical Research Council; JJ was an MRC PhD Scholar.

Abbreviations: aCSF, artificial cerebrospinal fluid; AP, action potential; 4-AP, 4-aminopyridine; DTx-I, dendrotoxin-I; TEA, tetraethylammonium; HaTx, hanatoxin; **MNTB, medial nucleus of the trapezoid body; VCN, ventral cochlear nucleus.**

References

Voltage (mV)	<i>mtau</i> (ms)	<i>ztau</i> (ms)	<i>N</i>
-37	0.62	10.01	2
-27	0.46	7.10	5
-17	0.41	5.79	5
-7	0.36	4.75	5
3	0.33	3.58	5
13	0.24	2.47	2

Table 1. Mean parameters of the Hodgkin-Huxley model fit to the isolated A-current.

	Calyceal synapse	Non-calyceal synapse
G_a (nS)	10	1.75
τ_{a1} (ms)	0.33	1
τ_{a2} (ms)	0.75	2
G_b (nS)	0.2	0
τ_{b1} (ms)	0.33	-
τ_{b2} (ms)	2.9	-

Table 2. Model parameters employed to generate synaptic conductances.

Figure 1. Properties of the A-current

A. Steady-state inactivation of the A-current was induced using the conditioning voltage steps displayed below the current traces. The peak current was measured on depolarization to -17 mV and is plotted against the conditioning voltage (part B, squares). **B.** Steady-state activation (circles) and inactivation (squares) curves (shown for one neurone) were normalized and fit with Boltzmann functions (grey lines). **C.** The A-current activation curve was obtained using a double test pulse protocol; T1 activates both transient and sustained currents, while T2 being preceded by a prepulse to -37 mV, only activates the sustained current. The peak A-current was measured in T1 and the current at the equivalent latency in T2 was subtracted to give the isolated A-current. (the dashed line indicates no change in the sustained current) **D.** The isolated A-current from the cell in C. **E.** To assess the rate of

recovery from inactivation, pairs of A-currents were elicited at different time intervals 0.5-240ms. A single exponential fit to the peaks of the second pulses (grey line). N.B. All data recorded in the presence of 3 mM TEA and 10 nM DTx-I

Figure 2. Pharmacology of the A-current

A. The A-current recorded at -7mV in the presence of 10nM DTx-I and 1mM TEA (black) with sequential application of 30mM TEA (grey) and 100mM TEA (light grey). Note that the A-current is still present even at 100mM TEA. **B.** The A-Current recorded at -7mV in the presence of 10nM DTx-I and 3mM TEA (black) with sequential application of 5mM 4-AP (grey). **C.** Application of 5 μM HaTx by puffer pipette reduces the magnitude of the A-current. The voltage protocol used is the same as figure 2 A. **D.** Voltage steps to -17mV from -107mV in the presence of TEA and DTx-I, in mouse (black) and rat (grey), note the absence of the A-current in the rat.

Figure 3. Kv4 expression in the MNTB

A. Examples of Kv4 immunoreactivity in the MNTB, for Kv4.1, Kv4.2 and Kv4.3. Insets show corresponding blocking peptide controls. Scale bar in Kv4.3 applies to all panels. The arrow in the left panel represents the orientation for all three panels. Bottom shows a single MNTB neuron stained with Kv4.3, the white arrow shows possible membrane localisation **B.** Kv4.3 shows robust staining while Kv4.2 and Kv4.1 are negligible. The brightness in (gray levels) of the MNTB was measured and divided by its blocking peptide control (n=3), dashed line represents non-specific background staining.

Figure 4. Model A-current.

A. A Hodgkin-Huxley model of the A-current (grey) is shown fit to data traces (black) from one MNTB neurone. B. The model A-current was derived from the mean activation and inactivation time constants from data in 5 neurones [see methods] and is shown here.

Figure 5. Responses of an MNTB model incorporating the model A-current

A. The voltage response to a simulated train of “calyceal” synaptic inputs is plotted with (black) and without (grey) the model A-current. B. An enlarged view of the first and last APs from part A, showing that the A-current makes a small contribution to repolarisation of the first AP. C. The magnitude of the A-current during the evoked response from part A. The voltage response to simulation of a small magnitude “non-calyceal” synaptic input with (D) and without (E) the A-current. F. The magnitude of the A-current during the evoked response from part D.

Figure 1.

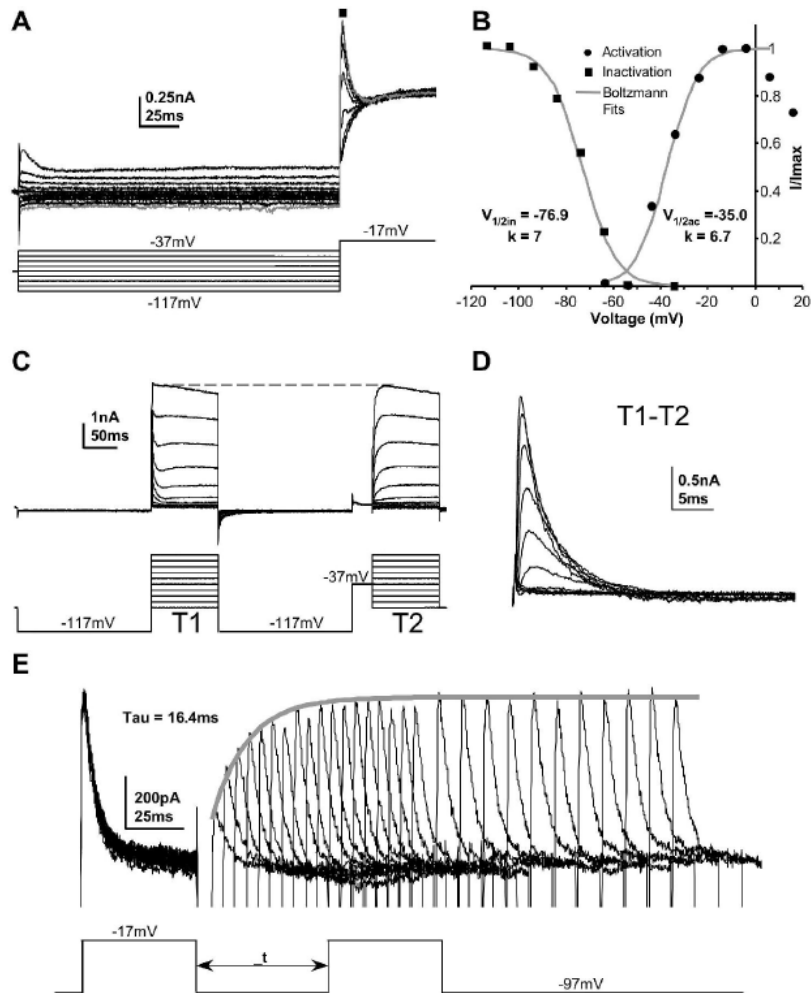


Figure 1. Properties of the A-current: A. Steady-state inactivation of the A-current was induced using the conditioning voltage steps displayed below the current traces. The peak current was measured on depolarization to -17 mV and is plotted against the conditioning voltage (part B, squares). B. Steady-state activation (circles) and inactivation (squares) curves (shown for one neurone) were normalized and fit with Boltzmann functions (grey lines). C. The A-current activation curve was obtained using a double test pulse protocol; T1 activates both transient and sustained currents, while T2 being preceded by a prepulse to -37 mV, only activates the sustained current. The peak A-current was measured in T1 and the current at the equivalent latency in T2 was subtracted to give the isolated A-current. (the dashed line indicates no change in the sustained current) D. The isolated A-current from the cell in C. E. To assess the rate of recovery from inactivation, pairs of A-currents were elicited at different time intervals 0.5-240ms. A single exponential fit to the peaks of the second pulses (grey line). N.B. All

Figure 2.

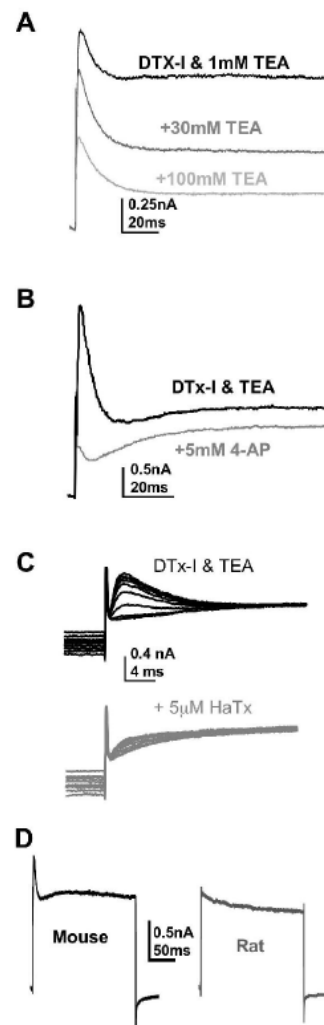


Figure 2. Pharmacology of the A-current: A. The A-current recorded at $\square 7\text{mV}$ in the presence of 10nM DTx-I and 1mM TEA (black) with sequential application of 30mM TEA (grey) and 100mM TEA (light grey). Note that the A-current is still present even at 100mM TEA. B. The A-Current recorded at $\square 7\text{mV}$ in the presence of 10nM DTx-I and 3mM TEA (black) with sequential application of 5mM 4-AP (grey). C. Application of $5\ \mu\text{M}$ HaTx by puffer pipette reduces the magnitude of the A-current. The voltage protocol used is the same as figure 2 A. D. Voltage steps to $\square 17\text{mV}$ from $\square 107\text{mV}$ in the presence of TEA and DTx-I, in mouse (black) and rat (grey), note the absence of the A-current in the rat.

353x1028mm (72 x 72 DPI)

Figure 3.

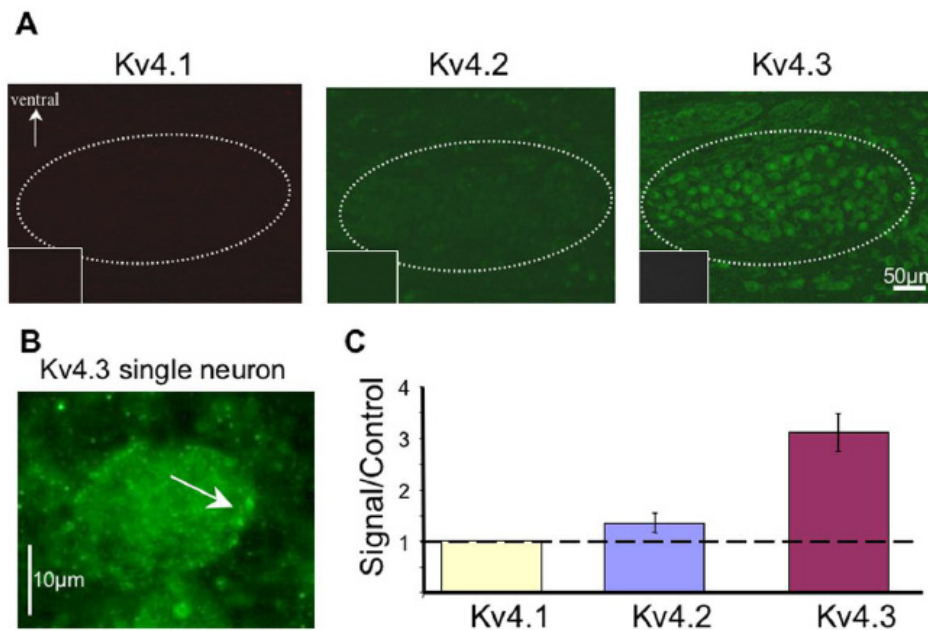


Figure 3. Kv4 expression in the MNTB A. Examples of Kv4 immunoreactivity in the MNTB (the extent of the nucleus is indicated by the dotted line), for Kv4.1, Kv4.2 and Kv4.3. Insets show corresponding blocking peptide controls. Scale bar in Kv4.3 applies to all panels. The arrow in the left panel represents the orientation for all three panels. B. A single MNTB neuron showing Kv4.3 immunolabelling. There are high levels of cytoplasmic staining and some plasma membrane staining (arrow) C. Kv4.3 shows robust staining while Kv4.2 and Kv4.1 are negligible. The brightness in (gray levels) of the MNTB was measured and divided by its blocking peptide control (n=3), dashed line represents non-specific background staining.

99x70mm (300 x 300 DPI)

Figure 4.

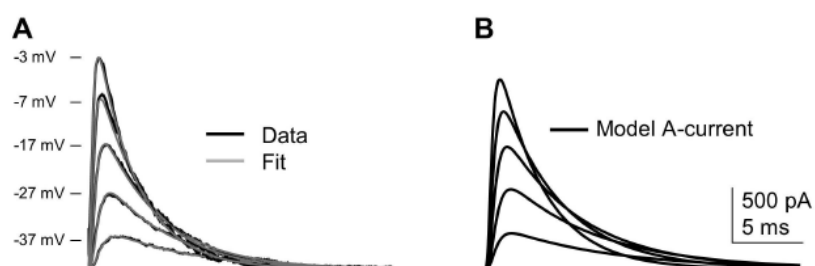


Figure 4. Model A-current: A. A Hodgkin-Huxley model of the A-current (grey) is shown fit to data traces (black) from one MNTB neurone. B. The model A-current was derived from the mean activation and inactivation time constants from data in 5 neurones [see methods] and is shown here.

Figure 5.

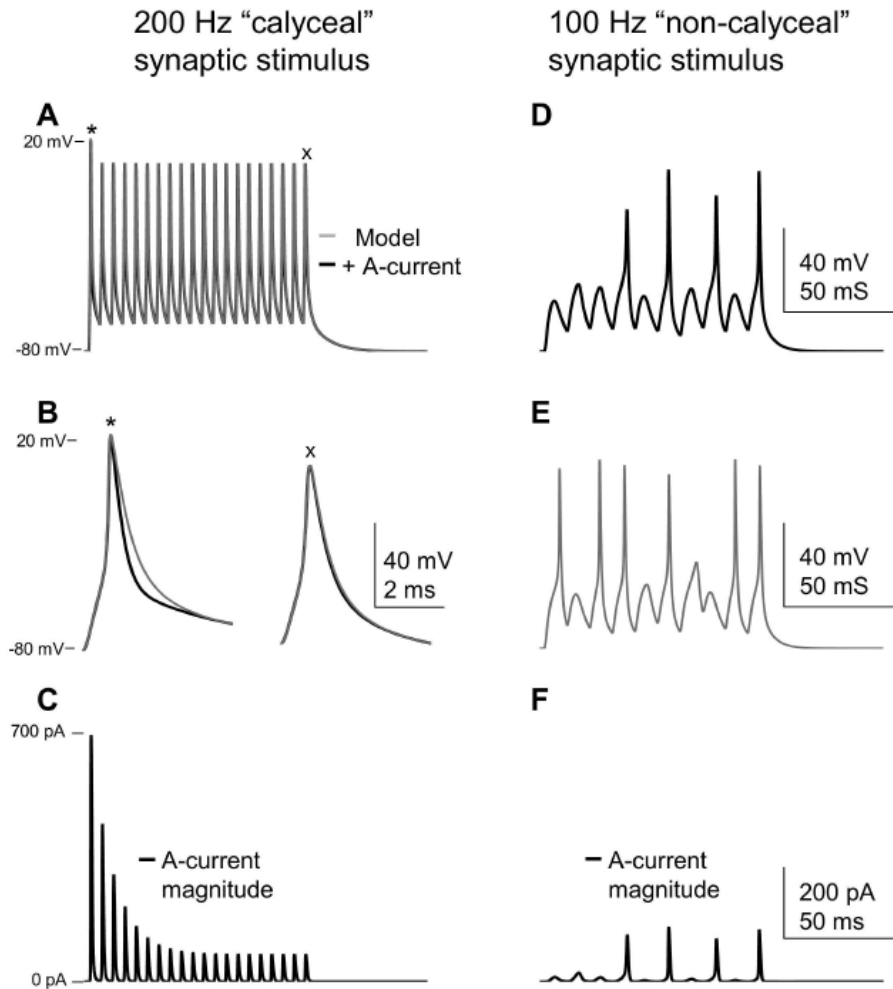


Figure 5. Responses of an MNTB model incorporating the model A-current: **A**. The voltage response to a simulated train of calyceal synaptic inputs is plotted with (black) and without (grey) the model A-current. **B**. An enlarged view of the first and last APs from part **A**, showing that the A-current makes a small contribution to repolarisation of the first AP. **C**. The magnitude of the A-current during the evoked response from part **A**. The voltage response to simulation of a small magnitude non-calyceal synaptic input with (**D**) and without (**E**) the A-current. **F**. The magnitude of the A-current during the evoked response from part **D**.